

Microscopic theory of the martensitic transition in *A-15* compounds based on a three-dimensional band structure*

R. N. Bhatt[†]

Department of Physics and Materials Research Laboratory, University of Illinois at Urbana-Champaign, Urbana, Illinois 61801 and Bell Laboratories, † Murray Hill, New Jersey 07974

(Received 14 February 1977)

A two-band tight-binding model of the electronic bands near the Fermi surface is formulated for the *A-15* compounds, based on Mattheiss's result that the density of states at the Fermi surface is composed mainly of the $\delta_1(x^2 - y^2)$ orbitals on the transition-metal sites. The model involves two tight-binding parameters (one intrachain and one interchain), one electron-phonon coupling constant and a bare elastic constant, and exhibits both an *X*-point Peierls gap and Jahn-Teller effects at a couple of saddle points in the bands, which are found to be jointly responsible for the instability of the electronic spectrum. For parameters determined by Mattheiss' calculation, and fits to the martensitic-transition temperature, specific heat at low temperatures, and $c_{11} - c_{12}$ above the transition, the model is able to predict the temperature variation of the susceptibility, distortion in the tetragonal phase, and the specific-heat jump at the transition. The results are in very good agreement with experiment for V_3Si , but not so good for Nb_3Sn , where because of the extremely short zero-temperature coherence length, lattice entropy, not included in the present model, could play a major part. A qualitative discussion of the softening of the shear modulus c_{44} , the marked softening of the [110] transverse $[\bar{1}\bar{1}0]$ polarized phonon away from $\vec{k} = 0$, and effects of non-transition-metal site alloying is included. Modifications of the highly successful Landau theory of the martensitic transition in *A-15* compounds by McMillan and the author, based on the Gor'kov model, are discussed in light of the present model and found to lead to no essential changes in its results.

I. INTRODUCTION

Much effort has gone into understanding the properties of the high-temperature superconducting *A-15* compounds (crystal structure shown in Fig. 1). Many of these compounds, like V_3Si and Nb_3Sn , in their purer forms are known to show structural instabilities and a martensitic transformation,¹ involving a cubic to tetragonal change in the unit cell and (sublattice) pairing of the transition-metal atoms on the faces of the unit cell (see Fig. 2), at a temperature T_m , before they become superconducting. Extensive experimental

data exist on all kinds of properties of these materials, particularly V_3Si ($T_m \sim 21$ K, $T_c \sim 17$ K) and Nb_3Sn ($T_m \sim 45$ K, $T_c \sim 18$ K), and more are available by the day, in the hope that these measurements will yield more clues as to the microscopic origin of the peculiarities that exist in these compounds.

Anomalous properties that characterize these compounds include: (i) Elastic softening as the temperature is lowered, particularly of the modulus ($c_{11} - c_{12}$), which becomes almost totally soft at T_m . The modulus c_{44} is more weakly dependent on temperature, while the bulk modulus ($c_{11} + 2c_{12}$) is essentially constant. (ii) The transverse [110]

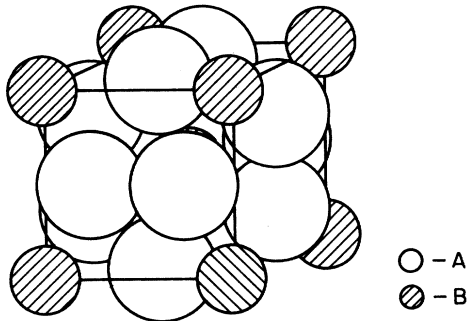


FIG. 1. *A-15* structure, A_3B . (Nontransition) atoms *B* form a bcc lattice and the (transition-metal) atoms *A* form three orthogonal chains along the cube faces with twice the periodicity of the lattice.

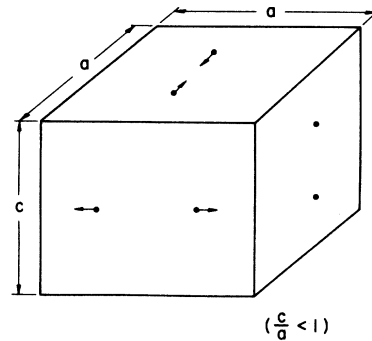


FIG. 2. Tetragonal phase in Nb_3Sn ($c/a < 1$). Cell distortion is accompanied by a $\Gamma_{12}^{(+)}$ sublattice distortion.

phonon with $[1\bar{1}0]$ polarization shows considerable softening with lowering of temperature, up to a substantial fraction of the way to the zone boundary. (iii) A divergent central peak is observed in neutron scattering experiments for the $[110]$ transverse $[1\bar{1}0]$ polarized phonon as the transition is approached from above; however, no pretransition (300) Bragg reflection corresponding to pairing of the transition-metal atoms is observed. (iv) Magnetic susceptibility increases as the temperature is lowered, and the Knight shifts are temperature dependent too. (v) The normal-state specific heat at low temperature has extremely large linear terms, indicating an anomalously large density of states at the Fermi surface. (vi) The temperature dependence of the resistivity of these compounds is rather unusual.

In almost all cases, there is a strong correlation between the anomalous properties and T_c : the greater the anomaly, the higher the superconducting temperatures. One exception is Nb_3Al , which, in spite of having $T_c = 18.5$ K, shows negligible temperature dependence of magnetic susceptibility and Knight shift, and a much smaller linear term in the specific heat; it does, however, show elastic softening, which is believed to be one of the reasons for the high T_c of these compounds. For further details, the reader is referred to the numerous review articles on the subject.²⁻⁵

Most microscopic theories attribute the anomalous properties to a large peak in the electronic density of states. In addition, the model must describe the mechanism by which the electrons drive the transition. In the original Labbe-Friedel model⁶ the martensitic transition is attributed to a second-order Jahn-Teller effect. Labbe and Friedel took a simple one-dimensional (1D) tight-binding model with the d orbitals of the transition-metal atoms which form linear chains on the faces of the cubic unit cell (Fig. 1), and include only nearest-neighbor (intrachain) coupling. The Fermi level was placed very close (~ 20 K) to the bottom of the d band (the point Γ in reciprocal space), where the three 1D bands due to the three orthogonal chains were degenerate, and the density of states had a $E^{-1/2}$ singularity. This degeneracy was removed by the tetragonal deformation with two of the bands moving together in one direction and the third moving twice as much in the opposite direction. In this noninteracting-chain model, no sublattice distortion was predicted and the shear modulus was predicted to be independent of temperature, both in disagreement with experimental results.

Soon afterward, Cohen, Cody, and Halloran (CCH)⁷ constructed an idealized model with a step-function density of states, put in a degeneracy splitting

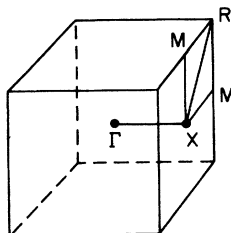


FIG. 3. Cubic Brillouin zone, showing the Γ , X, M, and R points.

exactly like the Labbe-Friedel model, and showed that essentially similar results were obtained by placing the Fermi energy close (~ 100 K) to the step in the electronic density of states. Since then, more refined versions of the Labbe-Friedel and the CCH model have been studied,⁸⁻¹⁰ including coupling to optical phonons. However, all these theories rely on a very sharp variation of the density of states, much sharper than is possible in a 3D band structure, with a consequent drop in density of states below the structural transition almost an order of magnitude larger than is actually indicated by the drop in magnetic susceptibility. In fact, Mattheiss' band-structure calculations¹¹ show that interchain coupling is strong enough that the 1D character of the bands is essentially wiped out; there is no threefold degeneracy in the bands at the Γ point near the Fermi energy, and therefore the Labbe-Friedel model is inappropriate.

The other major theory of the instability in the A-15 compounds is due to Gor'kov.^{12,13} The Gor'kov model of the martensitic transition is based on the Peierls charge-density-wave driven transition in a 1D chain. The model locates the Fermi energy close to the X point (center of the face of the cubic Brillouin zone—see Fig. 3), where by symmetry of the A-15 structure, two bands meet with opposite slopes of equal magnitude. This X-point degeneracy is removed by pairing of the transition-metal atoms in the linear chains, with a consequent lowering of energy if the Fermi level lies close to the X point. The pairing optical modes of the linear chains are coupled in turn to the strain tensor, and therefore the Gor'kov model leads to distortion of the unit cell as a secondary effect.

Gor'kov starts¹² with a model of three noninteracting orthogonal chains of transition-metal atoms. The temperature variation of the various elastic moduli follows directly from considerations of the crystal structure for various strains. A pure longitudinal $[100]$ strain causes a uniform compression of the $[100]$ chain of transition-metal atoms, while atoms in the $[010]$ and $[001]$ chains pair and depair, respectively (because of the coupling of the pairing optical modes to the lattice strain). This causes gaps to open in the elec-

tronic spectrum at the [010] and [001] X points and a (negative) logarithmic variation of the elastic constant c_{11} with temperature is indicated, as for the Peierls chain (see Ref. 14 for details). On the other hand, a uniform compressive stress causes no pairing, nor does a shear stress along one of the cube directions for noninteracting chains. Since no gaps open up, the bulk modulus $\frac{1}{3}(c_{11} + 2c_{12})$ and the shear modulus c_{44} are temperature independent in this approximation.

Thus for the Gor'kov model

$$\delta c_{12} = -\frac{1}{2}\delta c_{11} \sim \ln(\bar{\omega}/T), \quad (1)$$

where $\bar{\omega}$ is some cutoff energy of the order of the bandwidth, while δc_{44} is a measure of the interchain coupling.

To explain the temperature variation of the magnetic susceptibility, Gor'kov includes interchain coupling to essentially first order. For a pair of bands which are quite flat (to within ~ 1000 K) in the entire XMR plane with *no* dispersion along XM for one band, he obtains a density of states which has logarithmic singularities at the X and R points (such singularities are, of course, not present in Mattheiss' band structure or in a higher-order tight-binding calculation). For Gor'kov's band structure the variation in susceptibility in the cubic phase with temperature is logarithmic too.

Comparison between Gor'kov's theory and experiment yields reasonable agreement on the whole: the logarithmic terms describe the variation of the elastic constants and the magnetic susceptibility well over a large temperature range. The density of states determined from the fits is in agreement with experiment for V_3Si , but is too large for Nb_3Sn . The tetragonal distortion ($\epsilon = |c/a - 1|$) at zero temperature, *not correcting for the stabilization at T_c* , for the same values is 0.0037 for Nb_3Sn (experimental value 0.0062), and 0.0015 for V_3Si (experiment 0.0024). For Nb_3Sn the susceptibility drop below the transition is predicted to be more than twice the observed drop. One more disconcerting feature of the model is the extremely crucial placement of the Fermi energy, much like in the original Labbe-Friedel or the RCA models; a change of about 50–100 K would essentially wash out all the singularities. On the other hand, in the Gor'kov model the structural instability and superconductivity, both due to instability of the electron spectrum to opening of gaps at the Fermi surface, are intimately connected, and the transition temperatures are predicted to be of the same order of magnitude. For the Jahn-Teller models the instabilities are connected too; however, the proximity of the transition temperatures is essentially coincidental.

While Gor'kov's calculation is successful in ex-

plaining several phenomena associated with the martensitic transition in $A-15$ compounds, it is based on essentially a 1D band structure, which is not borne out by Mattheiss' band calculation. Consequently, a phenomenological Landau theory based on Gor'kov's picture of a charge-density-wave driven transition was developed by McMillan and the author¹⁵ (hereafter referred to as I), to test the model without making any inappropriate assumptions about the band structure. The calculation was successful in explaining almost all the major experimentally observed phenomena—the fits to both the [110] transverse and [100] longitudinal sound velocities were done with essentially one adjustable parameter, and with one more parameter—the coherence length—the [110] transverse-phonon curves were fit accurately at all temperatures for k halfway up to the zone boundary. Central peaks in neutron scattering and ultrasonic attenuation were shown not to follow from electron dynamics, and at least the former was in agreement with impurity scattering. Further, the heat capacity jump at T_m was in agreement with experiment using parameters determined by the low-temperature distortion. The (nonlinear) stress-strain curve just above the transition in V_3Si was adequately explained. The model showed a correlation between the sign of tetragonality and the effect of pressure on T_m and T_c , in agreement with the results for V_3Si and Nb_3Sn . The change in sign of tetragonality of Nb_3Sn with Sb alloying was accounted for. As demanded by the experimentally observed *absence* of (300) reflection above T_m , no optical mode was found to become soft. A calculation¹⁶ of the interplay between the charge-density-wave gap of the Gor'kov model and the BCS superconducting gap in V_3Si (where T_m is just above T_c) showed that the reduction in the electronic density of states due to the Peierls gap led to a 0.3-K reduction in T_c . Further, the onset of superconductivity arrested the growth of tetragonality as found experimentally, and for high-pressure (~ 25 kbar) it predicted that the martensitic transformation would be completely suppressed.

A few points, however, were not within the scope of the phenomenological theory—it did not explain the temperature variation of c_{44} , as interchain coupling was left out of the model, and this could be remedied. Further, it did not provide any information about the temperature variation of the magnetic susceptibility; indeed the only result it could yield in that respect was the drop in susceptibility below T_m , provided a correspondence was made between the parameters of the theory and those of a 1D Peierls model.¹⁴ There the effects were disastrous¹⁷: it predicted five times the

observed drop for Nb_3Sn , clearly indicating that such a correspondence was not correct and that 3D effects were important. Another result of the fit was that the zero-temperature coherence length in both Nb_3Sn and V_3Si , particularly the former, was very short and consequently the phonon softening extended way into the zone. For the Peierls chain the coherence length is related to the Fermi velocity; if such a correspondence was made the X -point velocity came out to be $\sim 2 \times 10^6$ cm/sec, which is so low that it essentially invalidates Gor'kov's assumption that the bands near the Fermi surface vary much more from Γ to X than in the XMR plane.

Recent augmented plane wave-linear combination of atomic orbitals (APW-LCAO) calculations of the band structures of a large number of $A-15$ compounds by Mattheiss¹¹ pose another problem for the Gor'kov model: they do not show any Gor'kov-like bands, which are flat in the XMR plane near the Fermi surface. What they do indicate, however, is that the density-of-states peak near E_F involves primarily transition-metal-atom d states with $\delta_1(x^2 - y^2)$ symmetry. Further, the calculation shows a set of two bands near the Fermi surface which is relatively isolated from the other bands for a large fraction of the Brillouin zone, except near the R point. The consistency with which Mattheiss finds the same bands near the Fermi surface for all the compounds studied leads one to the conclusion that any anomalies in the $A-15$ compounds which are electronic in origin should be due to these bands. However, Mattheiss' calculations are not much more precise than the width of the bands, and so details of the bands and the exact placement of the Fermi level within the band cannot be taken very seriously.

Consequently, in the present study a tight-binding model of the $A-15$ compounds is formulated from the δ_1 orbitals on the six transition-metal atom sites, including both nearest-neighbor (in-chain) and next-nearest-neighbor (interchain) interaction, and keeping only the two "relevant" bands. For interchain coupling less than about 15% of the nearest-neighbor interaction, the density of states has a sharp peak due to a couple of saddle points in the bands—one along ΓX for the upper band, and one at M for the lower band. A Fermi energy close to the peak would thus explain the large linear terms in specific heat at low temperatures. The model exhibits both a Peierls gap at the X point and a Jahn-Teller splitting at the M points for the lower band and at the ΓX saddle points for the upper band in the tetragonal phase with sublattice pairing. For interchain coupling of the magnitude given above, all these points are close to the Fermi level and

therefore both the Peierls gap and the Jahn-Teller splitting are jointly responsible for the electronic instability, and must both be taken into account.

The nearest-neighbor coupling has been taken to be within Mattheiss' rms error, while the next-nearest-neighbor coupling has been adjusted to give a reasonable fit to the low-temperature electronic specific heat. The overlap matrix elements (both nearest and next nearest neighbor) are assumed to vary linearly with the distance between the atoms, with a *single* phenomenological electron-phonon coupling parameter. Fitting the observed transition temperature and the elastic constant ($c_{11} - c_{12}$) in the cubic phase just above T_m determines both the "bare" elastic constant and the electron-phonon coupling constant. With no further adjustable parameters, the magnetic susceptibility, tetragonal distortion below T_m , and the specific-heat jump at the transition are predicted. The results are in good agreement with experiment for V_3Si ; for Nb_3Sn the agreement is not so good. Effects of (i) neglecting the lattice entropy, (ii) hybridization with other bands, and (iii) strong electron-phonon coupling taken into account only in a low-temperature limit in the present model are discussed, and (i) appears to be the cause of the few inadequacies of the model.

In order to present the essential physics of the Jahn-Teller effect shown by the bands (for the Peierls transition the reader may look up Ref. 14 or references contained therein), an idealized Jahn-Teller model with a more realistic density of states than the Labbe-Friedel or the CCH model for 3D bands is solved analytically in Sec. II; however, the results of this model necessarily bear only qualitative resemblance to the actual computer calculation for the tight-binding model. The tight-binding model is described in Sec. III, while Secs. IV and V include discussions of the calculational details and the results, respectively. The concluding Sec. VI summarizes the present state of affairs in the theory of $A-15$ compounds, and includes a discussion of the modification of the Landau theory of I in light of the present calculation.

II. IDEALIZED JAHN-TELLER MODEL

Of the idealized models exhibiting distortions due to a Jahn-Teller effect, the Labbe-Friedel⁶ 1D [$N(E) \sim E^{-1/2}$] and the CCH step-function density of states⁷ [$N(E) \sim \theta(E)$, as in the 2D free-electron case], have been used often in connection with the martensitic transition in the $A-15$ compounds. However, 3D densities of states do not exhibit such a singular variation, the sharpest variation being of the type \sqrt{E} , near an extremum or

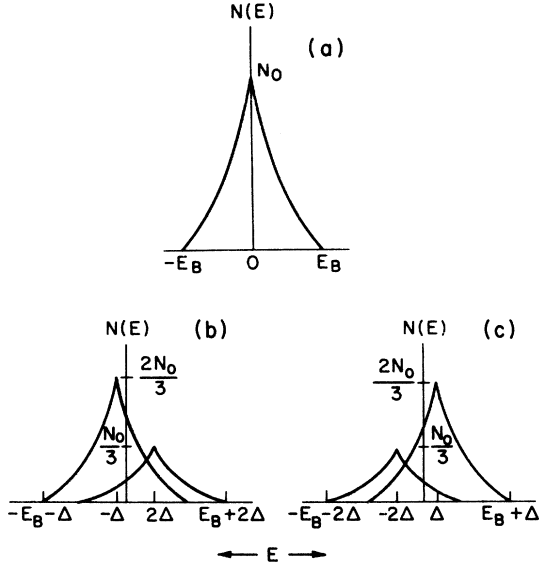


FIG. 4. Density of states for the idealized model for the cubic phase (a) and the two tetragonal phases (b, c).

a saddle point in the band. For the production of a large peak in the density of states, as indicated by specific heat^{18,19} and magnetic susceptibility^{20,21} data, two close-lying saddle points are required, and this is the case in the tight-binding model of the A-15 compounds to be discussed later.

To get an idea of the underlying physics, and the order of magnitude of the quantities involved, this section describes an idealized model exhibiting a second-order Jahn-Teller effect, which is one of the features of the tight-binding model.

The model consists of a density-of-states function composed of three terms:

$$N(E) = \sum_{i=1}^3 N_i(E), \quad (2)$$

where

$$N_i(E) = \begin{cases} \frac{1}{3} N_0 [1 - (|E - E_i|/E_B)^{1/2}], & |E - E_i| < E_B \\ 0, & |E - E_i| > E_B. \end{cases} \quad (3)$$

E_B is a measure of the width of this peaked density-of-states function.

Each of the three terms in this idealized model arise from a pair of saddle points of opposite nature at the energies E_i , which in the tight-binding model of the bands are the saddle points at M and along ΓX , for the three symmetry directions. The simplified model further puts the two saddle points at the same energy, and assumes that each pair moves together, dragging the entire density function with it, which is not true in the band-structure model. These points do have quantitative influences; however, the qualitative results of this

model are correct.

The three energies E_i , which are degenerate in the cubic phase, split in the tetragonal phase to (see Fig. 4):

$$E_1 = E_2 = +\Delta; \quad E_3 = -2\Delta, \quad (4)$$

where Δ is proportional to tetragonal strain. Δ may be either positive or negative, as will be seen later, so that the model allows for both kinds of tetragonalities. Near the transition temperature, all phonon coordinates which shift the electronic energy linearly or couple bilinearly to the tetragonal strain are simply proportional to each other, and so the elastic energy is proportional to Δ^2 .

The thermodynamic potential is given by

$$\begin{aligned} \Omega &= \Omega_{\text{elec}} + \Omega_{\text{elas}} \\ &= -\frac{1}{\beta} \sum_i \int N_i(E) \ln[1 + e^{\beta(\mu - E)}] dE + \frac{1}{2} K \Delta^2, \end{aligned} \quad (5)$$

where K is proportional to the unrenormalized shear modulus ($c_{11} - c_{12}$).

A. Landau expansion

To obtain the transition temperature and behavior at nearby temperatures, one may make a Landau expansion in powers of Δ . The expansion is complicated by the fact that for nonzero Δ , even for the Fermi level at zero, there is no electron-hole symmetry, and one has to keep track of the chemical potential. The first few terms may, however, be obtained in the following manner:

$$\left(\frac{\partial^2 F}{\partial \Delta^2} \right)_{\mathfrak{X}} = \left(\frac{\partial^2 \Omega}{\partial \Delta^2} \right)_{\mu} - \left(\frac{\partial^2 \Omega}{\partial \Delta \partial \mu} \right)^2 / \left(\frac{\partial^2 \Omega}{\partial \mu^2} \right)_{\Delta},$$

Thus,

$$\begin{aligned} \left(\frac{\partial^2 F}{\partial \Delta^2} \right)_{\mathfrak{X}} \Big|_{\Delta=0} &= K - \frac{2N_0}{T} \int_{-E_B}^{E_B} dE \left[1 - \left(\frac{|E|}{E_B} \right)^{1/2} \right] \\ &\quad \times e^{(E-\mu)/T} / (1 + e^{(E-\mu)/T})^2, \end{aligned}$$

and for the case $\mu = 0$ (for $\Delta = 0$, μ is independent of T at the peak), if $E_B > 5T$, the integrals may be extended to $\pm\infty$, and thus

$$\left(\frac{\partial^2 F}{\partial \Delta^2} \right)_{\mathfrak{X}} \Big|_{\Delta=0} \simeq K - 2N_0 [1 - 1.07(T/E_B)^{1/2}].$$

Consequently for $K < 2N_0$, the lattice is unstable in the undistorted configuration at a (Gaussian) temperature T_m^* given by

$$T_m^* \simeq 0.87 E_B (1 - K/2N_0)^2 \quad (6)$$

and

$$\frac{1}{2} \left(\frac{d^2 F}{d\Delta^2} \right)_{\mathfrak{X}} \Big|_{\Delta=0} \simeq \frac{1.07 N_0}{(E_B)^{1/2}} [T^{1/2} - (T_m^*)^{1/2}]. \quad (7)$$

At T_m^* , the coefficient of the cubic term is (except for terms involving $(\partial^2\Omega/\partial\Delta^2)_\mu$ and $(\partial\Omega/\partial\Delta)_\mu$ which vanish at $\Delta=0$, $T=T_m^*$)

$$\frac{1}{6} \left(\frac{\partial^3 F}{\partial \Delta^3} \right)_{\mathfrak{A}} \Big|_{\Delta=0} = \frac{1}{6} \left(\frac{\partial^3 \Omega}{\partial \Delta^3} \right)_{\mu} \Big|_{\Delta=0} \\ \sim \int_{-E_B}^{E_B} dE \left[1 - \left(\frac{|E|}{E_B} \right)^{1/2} \right] \\ \times \frac{e^{(E-\mu)/T} (1 - e^{(E-\mu)/T})}{(1 + e^{(E-\mu)/T})^3},$$

which changes sign as the Fermi level (at zero distortion) crosses the peak. Thus this model exhibits both signs of tetragonality, depending on the position of the Fermi level, much like the Landau theory of I. For $\mu=0$, the cubic term is zero, and the transition is second order. While this particular value of the chemical potential is an artifact of the symmetric density-of-states function, any density-of-states peak not too asymmetric will allow for both signs of tetragonality.

For the case $\mu=0$, because all the first three partial derivatives of the thermodynamic potential with distortion vanish at T_m^* , the coefficient of the quartic term is

$$\frac{1}{4!} \left(\frac{\partial^4 \Omega}{\partial \Delta^4} \right)_{\mu} \Big|_{\Delta=0} \simeq \frac{1}{24} \frac{12 N_0}{T^2} \int_0^\infty \left[1 - \left(\frac{T x}{E_B} \right)^{1/2} \right] \\ \times \frac{e^x (4e^x - e^{2x} - 1)}{(1 + e^x)^4} \\ \simeq 0.053 N_0 / (E_B T_m^*)^{1/2}, \quad (8)$$

which is positive, so that this model has no convergence problems present in the Labbe-Friedel model.²

The Landau expansion for the free energy for the half-filled band thus looks like

$$F = \frac{1.07 N_0}{(E_B)^{1/2}} [T^{1/2} - (T_m^*)^{1/2}] \Delta^2 + \frac{0.053 N_0}{(E_B T_m^*)^{1/2}} \Delta^4. \quad (9)$$

For T just below T_m^* , the distortion is

$$\Delta \simeq 2.26 T_m^* |\theta|^{1/2}, \quad (10)$$

where $\theta = (T - T_m^*)/T_m^*$ is the reduced temperature.

The jump in specific heat at the transition¹⁵ is thus

$$\Delta C_v \simeq 10 N_0 T_m (T_m/E_B)^{1/2}. \quad (11)$$

The magnetic susceptibility in the cubic phase, which is proportional to $(\partial^2\Omega/\partial\mu^2)_\Delta$, [Eqs. (5) and (25)] is

$$\chi \simeq \chi_0 [1 - 1.07(T/E_B)^{1/2}] \quad (T_m \leq T \ll E_B). \quad (12)$$

B. Analysis at zero temperature

At zero temperature the free energy is just the total energy, and may be calculated directly. However, it may also be obtained from the thermodynamic potential in the following manner:

$$\left(\frac{\partial F}{\partial \Delta} \right)_{\mathfrak{A}} = \left(\frac{\partial \Omega}{\partial \Delta} \right)_{\mu} \\ = \frac{N_0}{3} \int_{-E_B}^{E_B} dE \left[1 - \left(\frac{|E|}{E_B} \right)^{1/2} \right] \\ \times \left(\frac{2}{1 + e^{\beta(E+\Delta-\mu)}} - \frac{2}{1 + e^{\beta(E-2\Delta-\mu)}} \right) + K \Delta,$$

which for $T=0$ reduces to

$$\left(\frac{\partial F}{\partial \Delta} \right)_{\mathfrak{A}} = -\frac{2}{3} N_0 \int_{\mu-\Delta}^{\mu+2\Delta} dE \left[1 - \left(\frac{|E|}{E_B} \right)^{1/2} \right] + K \Delta.$$

Consider only $\Delta > 0$ (the analysis for $\Delta < 0$ is similar). If $\mu < \Delta$ then

$$\left(\frac{\partial F}{\partial \Delta} \right)_{\mathfrak{A}} = (K - 2N_0)\Delta \\ + \frac{4N_0}{9(E_B)^{1/2}} [(\Delta - \mu)^{3/2} + (\mu + 2\Delta)^{3/2}].$$

For the case of a half-filled band, electron number conservation implies

$$N = N_0 \int_{-E_B}^0 \left[1 - \left(\frac{|E|}{E_B} \right)^{1/2} \right] dE \\ = \frac{N_0}{3} \left\{ \int_{-E_B}^{\mu-\Delta} 2 \left[1 - \left(\frac{|E|}{E_B} \right)^{1/2} \right] dE \right. \\ \left. + \int_{-E_B}^{\mu+2\Delta} \left[1 - \left(\frac{|E|}{E_B} \right)^{1/2} \right] dE \right\}$$

or

$$\mu = [2/9(E_B)^{1/2}] [(2\Delta + \mu)^{3/2} - 2(\Delta - \mu)^{3/2}], \\ \Rightarrow \mu \simeq [4(\sqrt{2} - 1)/9(E_B)^{1/2}] \Delta^{3/2}, \quad (13)$$

where Δ has been assumed much smaller than E_B . Thus μ is much smaller than Δ , and keeping the leading two orders in the expansion

$$\left(\frac{\partial F}{\partial \Delta} \right)_{\mathfrak{A}} \simeq (K - 2N_0)\Delta + \frac{4(2\sqrt{2} + 1)}{9} \frac{N_0}{(E_B)^{1/2}} \Delta^{3/2},$$

or

$$F = -1.07 N_0 (T_m^*/E_B)^{1/2} \Delta^2 \\ + 0.68 [N_0/(E_B)^{1/2}] \Delta^{5/2}, \quad (14)$$

which has a minimum at

$$\Delta_0 \simeq 1.6 T_m^*. \quad (15)$$

As assumed earlier, Δ_0 is much less than E_B .

Neglecting the variation in chemical potential,

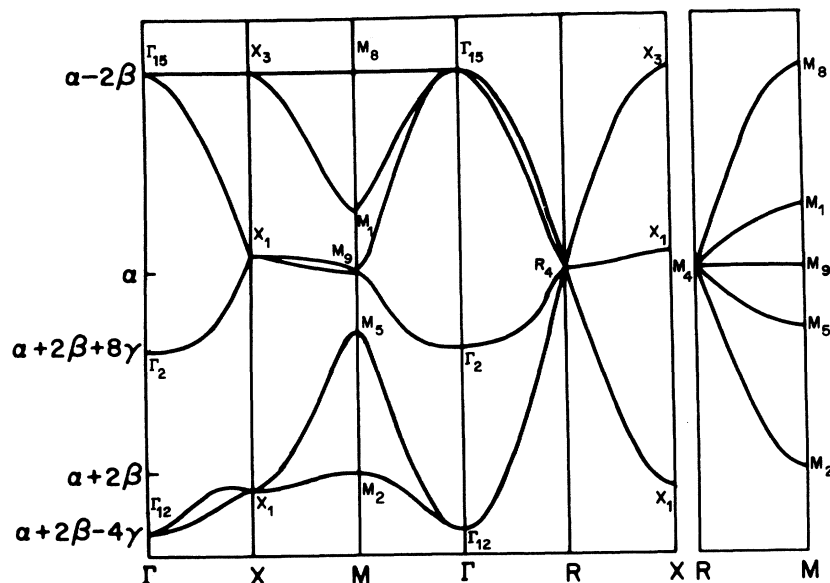


FIG. 6. Six tight-binding bands for typical values of the parameters ($\beta < 0$, $\gamma = -0.15\beta$).

composed mainly ($\sim 50\%$) of the $\delta_1(x^2 - y^2)$ subband with about 25% contribution from the $\pi(xz, yz)$ orbitals and the rest a mixture of other states. (iii) The bands near the Fermi surface are almost an order of magnitude less flat than that required by Gor'kov in the entire zone face (XMR); consequently the phase space involved is too small for a Peierls-like effect to be the sole cause of the distortion.

The band structure of Mattheiss shows a set of two bands close to the Fermi surface in all the compounds, which are reasonably isolated for most of the Brillouin zone. These are composed, as stated above, mainly of the δ_1 orbitals on the transition-metal sites. The consistency with which the same two bands lie near the Fermi surface for all the compounds in Mattheiss' study shows that this result is relatively insensitive to the lattice potential and is therefore strong evidence for these bands being responsible for any electronic instabilities in the A-15 compounds. In this study, therefore, a simplified tight-binding model of these two bands has been taken, composed of only the δ_1 orbitals on the six A sites, and including nearest-neighbor (intrachain) and next-nearest-neighbor (interchain) coupling. Coupling to the B atoms has not been included. The model is partly phenomenological; this has been necessitated by the fact that while Mattheiss' identification of the bands near the Fermi surface is reliable, his tight-binding parameters for the δ_1 orbital are within the rms deviation of his LCAO fit to the APW results, and consequently not reliable. Thus the nearest-neighbor coupling is taken such that the band separation is within his rms errors, and

the next-nearest-neighbor coupling has been adjusted to give a peak in the density of states somewhat larger than the density of states at the Fermi surface inferred from experimental data on specific heat. The variation of all the matrix elements (both nearest-neighbor and next-nearest-neighbor) is accounted for by a single phenomenological parameter g , and taken to be of the form

$$M_{ij}(d) = M_{ij}(0)(1 - gd), \quad (17)$$

where d is the change in direct (straight-line) distance between the atoms. This would be true if the exponential factors in the tight-binding wave functions were the dominant variation, or if variation in either the nearest- or next-nearest-neighbor coupling dominated the other. Neither of these is completely true for the A-15 compounds, so Eq. (17) should be regarded as a further simplification of the model. To do a better job would require more adjustable parameters, and such a procedure is probably not warranted in view of the original simplicity of the model.

In terms of the diagonal element α , nearest-neighbor coupling β , and the next-nearest-neighbor constant γ (in the cubic phase), the optical mode amplitude d_0 , and the tetragonal distortion d_T , the 6×6 tight-binding matrix becomes of the form shown in Table I. The wave vector \vec{k} has been written in dimensionless form, so that the Brillouin zone edges are at $(\pm\pi, \pm\pi, \pm\pi)$ in both the cubic and the tetragonal phases. The variation of the diagonal matrix element α due to change in lattice potential as a result of the distortion has been dropped, as this would just give an overall (k -independent) shift in the bands, which can be

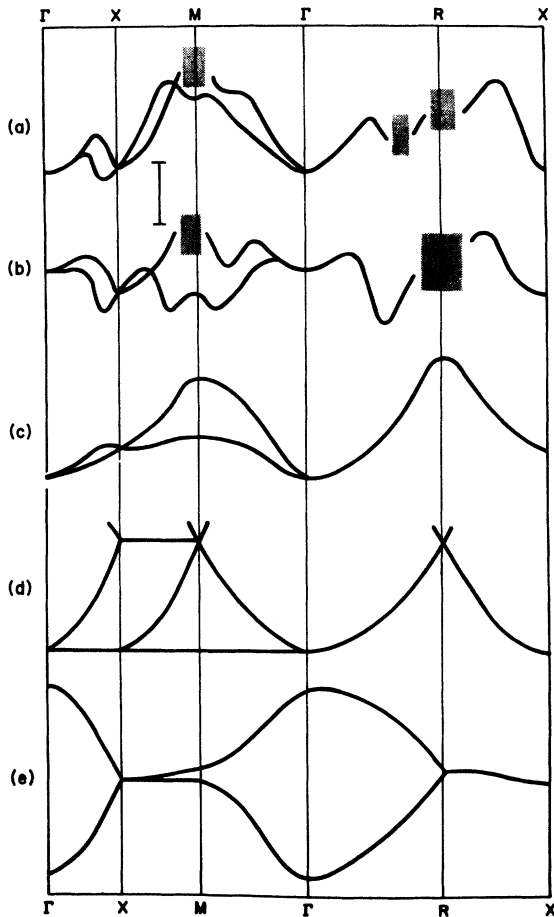


FIG. 7. Two bands near the Fermi surface in Mattheiss, calculation for Nb_3Sn (a) and V_3Si (b), along with the bands used in the present calculation (c), the Labbe-Friedel model (d), and the Gor'kov model (e), drawn roughly to scale. The shaded area in Mattheiss' band represents presence of other bands (and consequent mixing), and his rms error is indicated by I.

absorbed into the elastic term.

The bands in the cubic phase for $\beta < 0$ (as per Mattheiss' values) and $\gamma > 0$ (a choice necessary to make the bands look like those of Mattheiss) are shown in Fig. 6. The bands of relevance are the two lowest ones which are degenerate along ΓR and XR . At Γ , these are split off from the nearest band by an amount 12γ , while at R all the six bands meet, as in the linear-chain model. For most of the zone, however, the other bands are far separated, and may therefore be omitted from the discussion. The degeneracy at Γ and at two of the three X points is removed by the tetragonal distortion, or the pairing optical model. The density of states near the Γ point is three dimensional (i.e., $N(E) \sim \sqrt{E}$) for any reasonable value of γ , and therefore the Labbe-Friedel model is

not appropriate. The X -point model of Gor'kov is in somewhat better shape; but, like in Mattheiss' calculation, the bands are about an order of magnitude wider than required by Gor'kov on the zone face XMR (the middle two bands are more appropriate for a pure Peierls-like instability), and so the objection raised before holds.

However, for $\gamma < 0.15\beta$, the points X and M for the lower band are close in energy (splitting $\sim \gamma^2/\beta$) and the density of states has a sharp peak due to the saddle points at M in the lower band, and the one between Γ and X in the upper band. These saddle points shift when a tetragonal distortion occurs (the saddle points for two symmetry directions moving one way and for the third the other way), while gaps open up at two of the X points. Therefore, the tight-binding band model is capable of exhibiting an electronic instability which can be attributed partly to a Jahn-Teller effect, and partly to a Peierls gap mechanism.

A comparison between various models can be made by looking at the band structure responsible for the electronic instability in each of the models. This is done in Fig. 7 where the electronic bands near the Fermi surface have been plotted for the Labbe-Friedel, the Gor'kov and the present models, along with the best LCAO fits by Mattheiss to his APW results. As can be seen, the bands of Mattheiss do not resemble those of Gor'kov at all; the Labbe-Friedel model, on the other hand, has bands which are perfectly flat in the ΓXM plane, which is unrealistic. The bands of the present tight-binding model, however, do not have perfectly flat portions; further, they bear a reasonable resemblance to Mattheiss' best fits. While doing this comparison it should be kept in mind that Mattheiss' rms error (shown in Fig. 7) is comparable to the width of these bands, and so many of the features of Mattheiss' bands are not reliable. It seems quite clear that the present 3D band model is much more realistic than the idealized models of Labbe-Friedel and Gor'kov, which have perfectly flat portions due to the (probably quite misleading) one dimensionality of the bands. Consequently the results based on the present model are likely to have a much closer bearing on the actual situation in the $A-15$ compounds. Besides having a 3D character, the present model is simple enough that its few parameters are easily fixed up by Mattheiss' calculation coupled with a few experimental results, and predictions of other quantities can be made.

IV. DETAILS OF THE CALCULATION

In order to deal with a problem involving two energy scales — a bandwidth $\sim 10^4$ K and a transition temperature $\sim 20-50$ K — it becomes necessary

to divide the Brillouin zone into regions which are dealt with in two radically different ways. The first is the bulk of the Brillouin zone where energy variations are large and which contributes a fraction of the density of states at the Fermi surface which is not sensitive to small dilations of the lattice structure. This region has been divided into cubes, each with a side $\frac{1}{15}$ to $\frac{1}{20}$ of the Brillouin-zone half length π . The constant energy surfaces have been approximated by planes within each cube, using an averaged linear interpolation scheme, which uses the energy eigenvalues at all eight corners of the cube. The density of states for this case has been worked out by Gilat and Raubenheimer,²² and the relevant formulas are summarized in the Appendix. Since the energy variation is greater than the temperature by a factor ~ 10 within each cube, low-temperature expansions of the thermodynamic functions can be used.

For the special regions which are comprised of (i) the region surrounding the XM line for the lower band, and (ii) the region from X to the saddle point along ΓX for the upper band, which are reasonably flat and near the Fermi energy, use has been made of a finer mesh for interpolating the energy eigenvalues, and usual thermodynamic formulas have been used to evaluate the free energy and its derivatives. Since the thermodynamic functions are sharply peaked, a large number of points ($\sim 25\,000$) have been used for the integration (changing the number of points by a factor of 2 does not alter the final results by more than a few percent) and all derivatives taken analytically; even the specific heat is obtained by a least-squares fit to the entropy by a power series, and then analytically differentiating the series.

The energy eigenvalue at each mesh point has been represented by a power series up to cubic terms in the tetragonal distortion. The bands at an arbitrary point in the zone vary linearly for small distortion, while the free energy itself is quadratic because different portions of the Brillouin zone move in a correlated manner (the points in the star of the cubic Brillouin zone move such that the sum of their linear motion is zero). In order that this enormous cancellation is exact, the linear terms in the power series have to be evaluated in double precision, using extremely small distortion, about 10^{-4} – 10^{-5} of the actual distortion. The remaining two terms (quadratic and cubic) in the expansion have been obtained by a least-squares fit of the energy eigenvalues for distortions up to about twice the zero-temperature distortion. This is somewhat in error near degeneracy points where non-power-law terms like $(\epsilon^2 + \Delta^2)^{1/2}$ are present; however, the X -point re-

gion where this really matters is small, and the net error is not consequential.

A. Thermodynamic formulas

It is convenient to work with the thermodynamic potential $\Omega(T, \Delta, \mu)$ instead of the free energy $F(T, \Delta, \mathcal{N})$. (Since the volume change at the transition is second order in the dilatation, the volume will be taken to be a constant and suppressed as a thermodynamic variable.) The thermodynamic potential is the sum of the electronic and elastic parts:

$$\Omega = -\frac{1}{\beta} \sum_{n=1}^2 \sum_{\mathbf{k}} \ln(1 + e^{-\beta LE_{\mathbf{k}}^n(\Delta) - \mu(\Delta)}) + \frac{1}{2} K \Delta^2, \quad (18)$$

where the sum is over the two bands n and the Brillouin zone and Δ represents the distortion of the crystal. ($\beta = 1/T$; $k_B = 1$.) K is proportional to the elastic constant. The lattice entropy has not been included in Eq. (18) as its effects have so far been believed to be small (this point will come up later in the discussion).

The electron number and derivative of the free energy (at constant electron number) are simply the partial derivatives of the thermodynamic potential

$$\mathcal{N} = -\left(\frac{\partial \Omega}{\partial \mu}\right)_{\Delta, T}, \quad (19a)$$

$$\left(\frac{\partial F}{\partial \Delta}\right)_{T, \mathcal{N}} = \left(\frac{\partial \Omega}{\partial \Delta}\right)_{T, \mu}. \quad (19b)$$

Thus the minimum of the free energy is given by the zero of the latter equation. The curvature at the minimum (proportional to the elastic constant) is related by the thermodynamic relation

$$\left(\frac{\partial^2 F}{\partial \Delta^2}\right)_{T, \mathcal{N}} = \left(\frac{\partial^2 \Omega}{\partial \Delta^2}\right)_{T, \mu} - \left(\frac{\partial^2 \Omega}{\partial \Delta \partial \mu}\right)_T^2 / \left(\frac{\partial^2 \Omega}{\partial \mu^2}\right)_{T, \Delta}. \quad (19c)$$

Other quantities of interest are the free energy, entropy, and the specific heat:

$$F = \Omega + \mu \mathcal{N}, \quad (20a)$$

$$S = -\left(\frac{\partial \Omega}{\partial T}\right)_{\Delta, \mu}, \quad (20b)$$

$$C = T \left(\frac{\partial S}{\partial T}\right)_{\mathcal{N}}. \quad (20c)$$

In Eq. (20c), Δ has to be allowed to vary to equilibrium, given by the zero of Eq. (19b).

For the bulk of the Brillouin zone, where low-temperature expansion has been used, the electronic part of the thermodynamic potential may be expressed as the power series

$$\frac{\Omega_{\text{elec}}}{V} = \int_0^{\mu(\Delta)} N_{\Delta}(E)[E - \mu(\Delta)] dE - \frac{1}{6}\pi^2 T^2 N(\mu) - \frac{7}{360}\pi^4 T^4 N''(\mu) - \dots, \quad (21)$$

where $N(\mu)$ is the density of states at the Fermi surface.

Derivatives with respect to μ and T may be taken in a straightforward manner. In taking the derivative with respect to Δ , it has been assumed that within each cube the change of energy is constant, so that it may be replaced by $(dE_c/d\Delta)$ where E_c is the energy at the center of the cube. In this way, from Eq. (18) it follows that

$$\frac{\partial}{\partial \Delta} \simeq - \left(\frac{dE_c}{d\Delta} \right) \frac{\partial}{\partial \mu}. \quad (22)$$

The calculation for each point or cube was done in single precision and the results added in double precision, ensuring six or seven figures of final accuracy. In the computation of the free energy, because of the large constant contribution from the Fermi sea in the bulk of the Brillouin zone, the changes are obscured by noise, and Eq. (20a) had to be modified to remove the large background. The density of states $N_{\Delta}(E)$ was expanded in powers of Δ , assuming that for each cube, the only variation of $N_{\Delta}(E)$ is through the variation of the energy at the center, E_c (which is equivalent to the assumption of constant change of eigenvalues within each cube) so that

$$N_{\Delta}(E) \simeq N_0(E) + \left(\frac{dN}{dE_c} \right)_{E_c} (E_c - E_c^0) - \frac{1}{2} \left(\frac{d^2N}{dE_c^2} \right)_{E_c} (E_c - E_c^0)^2,$$

where E_c is the energy at the cube center in the distorted configuration and the sign of the last term is different from the usual Taylor expansion because the derivatives are taken at E_c , not E_c^0 . Using $dN/dE_c = -(dN/dE)$ (i.e., raising the energy at the center of the cube is equivalent to taking the density of states at a lower energy in the original configuration), the large contribution to the free energy per unit volume becomes

$$\begin{aligned} \frac{F_1}{V} &= \int_{-\infty}^{\mu} N_{\Delta}(E) E dE \\ &= \int_{-\infty}^{\mu} E [N_0(E) - \delta E_c N'_{\Delta}(E) - \frac{1}{2} (\delta E_c)^2 N''_{\Delta}(E_c)] dE \\ &= \int_{-\infty}^{\mu_0} E N_0(E) dE \\ &\quad + \int_{\mu_0}^{\mu} E [N_{\Delta}(E) + \delta E_c N'_{\Delta}(E) + \frac{1}{2} (\delta E_c)^2 N''_{\Delta}(E)] dE \\ &\quad - \int_{-\infty}^{\mu} E [N'_{\Delta}(E) \delta E_c + \frac{1}{2} N''_{\Delta}(E) (\delta E_c)^2] dE, \end{aligned}$$

where $\delta E_c = E_c - E_c^0$, and μ_0 is a fixed reference point (independent of Δ and T), chosen close to μ , so that the second integral may be evaluated by expanding the integrand about $E = \mu$. After some algebra one obtains

$$\begin{aligned} F_1/V &= F_1^0/V + \left[\frac{1}{2} \mu^2 N_{\Delta}(\mu) - \frac{1}{6} \mu^3 N'_{\Delta}(\mu) + \frac{1}{24} \mu^4 N''_{\Delta}(\mu) \right] \\ &\quad + \delta E_c [n_{\Delta}(\mu) - \mu N_{\Delta}(\mu) + \frac{1}{2} \mu^2 N'_{\Delta}(\mu) - \frac{1}{6} \mu^3 N''_{\Delta}(\mu)] \\ &\quad + \frac{1}{2} (\delta E_c)^2 [N_{\Delta}(\mu) - \mu N'_{\Delta}(\mu) + \frac{1}{2} \mu^2 N''_{\Delta}(\mu)], \quad (23) \end{aligned}$$

where $F_1^0 = \int_{-\infty}^{\mu_0} E N_0(E) dE$ is a large constant contribution to F_1 , which may be neglected; $n_{\Delta}(E) = \int_{-\infty}^E N_{\Delta}(E) dE$ is the number of electrons below E for a distortion Δ ; and μ_0 has been chosen to be the zero point of energy. Only up to second derivatives of $N_{\Delta}(\mu)$ have been kept, since in the plane energy surface approximation the third derivative is zero.

The calculation was done starting at the lowest temperatures in the tetragonal phase. The number of electrons was chosen so that the Fermi level was close to the peak in the density of states and the bare elastic constant adjusted so that the transition temperature agreed with experiment. The equilibrium state, defined by Eq. (19a) and the zero of Eq. (19b) was obtained using a linear interpolation procedure in the $\mu - \Delta$ plane involving the first and second derivatives of the thermodynamic potential. Convergence was usually obtained in less than five iterations starting from an educated (~20%) guess, except near the transition, where it had to be stopped from locking onto the cubic phase. The various thermodynamic functions, elastic constants, and susceptibility were calculated using the formulas given. The transition temperature was obtained by determining the free energy in the cubic and tetragonal phases at various temperatures and finding the intersection of third- or fourth-order polynomial (in temperature) fits to the two functions $F_{\text{cub}}(T)$ and $F_{\text{tet}}(T)$.

B. Strong-coupling enhancement

It is well known²³ that strong electron-phonon coupling enhances the electronic specific heat in the normal state at low temperatures by a factor $(1 + \lambda)$, where λ is the electron-phonon coupling constant. This is due to a renormalization of the electronic spectrum (and consequently the density of states) within an energy of the order of the Debye temperature Θ_D of the Fermi surface. This factor is strictly valid only at low temperatures and is washed out by thermal effects when T becomes a sizable fraction of Θ_D . Since the enhancement is "stuck" to the Fermi surface, at low temperatures the effect of strong electron-phonon coupling on the free energy of the system may be taken into consideration by multiplying the

thermodynamic factors by a function $f(E - \mu)$ which satisfies

$$\begin{aligned} f(0) &= 1 + \lambda \\ \text{and} \quad & \\ f(\pm\infty) &= 1, \end{aligned} \quad (24)$$

with a characteristic variation over a range $\sim \Theta_D$. Then

$$\begin{aligned} \Omega &= -\frac{1}{\beta} \int dE N(E) \ln(1 + e^{-\beta(E-\mu)}) \\ &\rightarrow -\frac{1}{\beta} \int dE N(E) f(E-\mu) \ln(1 + e^{-\beta(E-\mu)}), \\ \mathcal{H} &= \int dE \frac{N(E)}{1 + e^{\beta(E-\mu)}} + \int dE \frac{N(E)f(E-\mu)}{1 + e^{\beta(E-\mu)}} \text{ etc.} \end{aligned}$$

With these replacements it is easily seen that if the density of states is relatively constant over Θ_D , then the zero-temperature energy is barely changed by the modification. On the other hand, the electronic entropy at low temperatures, which depends only on an integral over a region $\sim T (\ll \Theta_D)$ around the Fermi surface, is renormalized by a factor $(1 + \lambda)$, as is specific heat. The same follows for the temperature variation of the elastic constants and magnetic susceptibility, which are due to a reshuffling of the electron population over a region of width T around the Fermi surface. Thus for a density-of-states function not varying much over a range Θ_D , the zero-temperature quantities—zero-temperature energy, magnetic susceptibility, and elastic constants—are dependent on the bare density of states, while for low temperature, the temperature-dependent quantities—entropy, specific heat, temperature dependence of elastic constants, and magnetic susceptibility—are enhanced by a factor $(1 + \lambda)$.

If, in addition, the density of states is sharply varying over a range $\sim \Theta_D$ (as is probably true in the A-15 compounds), then even the zero-temperature quantities depending on the Fermi surface, like zero-temperature magnetic susceptibility, will be renormalized too—by as much as $(1 + \lambda)$ in the extreme case. *This has been assumed in the present study*; however, this last assumption affects only the absolute level of the magnetic susceptibility curve, which is not well known theoretically and has been adjusted to agree with experiment.

Clearly, a better job would require an elaborate self-consistent treatment involving strong coupling superconductivity for a peaked density of states exhibiting both Jahn-Teller and Peierls instabilities, which is a formidable task.

V. RESULTS AND DISCUSSION

The tight-binding model described in Sec. III has been used to study the structural phase transition and anomalous properties of Nb_3Sn and V_3Si . The nearest-neighbor coupling obtained from Mattheiss' LCAO fit to the δ_1 band are -0.37 and -0.44 eV, respectively, which are quite small and consequently not very reliable. An estimate of the error may be made by looking at the separation of the peaks in the density of states of the δ_1 orbitals by Mattheiss and his rms error of about 0.3 eV; the result is that the nearest-neighbor couplings could be wrong by as much as 50%.

Two sets of nearest-neighbor parameters β have been chosen for each case, V_3Si and Nb_3Sn , within the limits of Mattheiss' accuracy. The next-nearest-neighbor parameter (γ) has been adjusted so as to give a rough agreement with experimental results on specific heat along with reasonable predictions regarding the variation of elastic constant, magnetic susceptibility, and tetragonal deformation with temperature, and the specific heat jump at the transition. *No elaborate fitting attempt has been made, however, and the parameters chosen are representative, not best fits.*

The position of the Fermi level has been chosen to be close to the peak in the density of states, where the transition temperature is the largest and the elastic constant K is adjusted to yield the right transition temperature. The transition is second order for only a special placement of the Fermi energy, which is difficult to achieve; consequently, weakly first-order transitions have been accepted.

The free energy, entropy, and specific heat in the two phases (schematic diagram in Fig. 8) have been calculated as described in Sec. IV, along with the deformation below the transition, elastic constant ($c_{11}-c_{12}$) in the cubic phase, and magnetic susceptibility. The magnetic susceptibility is given by

$$\chi(T) = (1 + \lambda) \mu_B^2 \int d\epsilon N_\Delta(\epsilon) \left(-\frac{\partial f}{\partial \epsilon} \right) + \chi_{\text{background}}, \quad (25)$$

where f is the Fermi function $f(\epsilon) = (1 + e^{\beta[\epsilon - \mu(\Delta)]})^{-1}$, $N_\Delta(\epsilon)$ is the density of states for both bands and $\chi_{\text{background}}$ is a temperature-independent background due to other bands and diamagnetic effects, presumably much smaller than the contribution from the two bands under consideration. As stated earlier the strong coupling factor $(1 + \lambda)$ has been included to give the correct temperature dependence of $\chi(T)$; any error in $\chi(T=0)$ due to this is absorbed into the background term. Electron-electron enhancement effects, on the other hand, have been left out of Eq. (25), as the data seem to

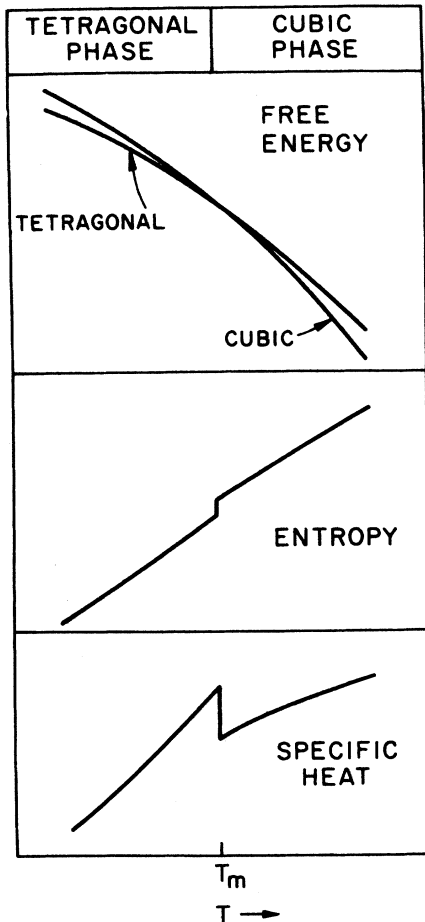


FIG. 8. Schematic plot of the free energy, electronic entropy, and electronic specific heat as functions of temperatures for a weakly first-order transition.

be better fit without them.

The calculation is valid only for reasonably low temperatures, because of (i) low-temperature expansion in the bulk of the Brillouin zone, (ii) assumption of a temperature-independent proportionality between the optical mode, tetragonal distortion, and electronic coordinates which is valid near the transition only, and (iii) enhancement due to strong electron-phonon coupling, which is constant only for $T \ll \Theta_D$, the Debye temperature.

The elastic constant ($c_{11}-c_{12}$) is determined within a factor and the factor has been adjusted to give the correct slope at the transition temperature; this determines the low-temperature distortion ($c/a - 1$). Since the elastic constant is essentially linear for temperatures where the calculation is valid, it has not been plotted with the other quantities to show agreement with experiment.

For Nb_3Sn the ratio of the sublattice distortion

to the tetragonal deformation has been measured²⁴; the relative sign was not certain and the sign which gives a larger gap at the X point (the motion of the lower band at the M point is independent of the optical mode), shown in Fig. 2 has been used. For V_3Si experimental data on the magnitude of the sublattice distortion is inadequate¹⁵ and so the same ratios have been used; if the M -point motion is more important than the Peierls gap at the X point, as appears to be the case in the present model, this will cause only a slight quantitative difference in the results (probably less than 5%–10%).

The parameters for the different cases, along with the results, have been given in Table II. The two bands have been drawn for case I used in V_3Si and Nb_3Sn , which are just scaled (1:1.5) versions of one another (Fig. 9). The density of states for the four cases are shown in Fig. 10. The specific heat, susceptibility, and temperature variation of the tetragonal distortion for the first case in both V_3Si and Nb_3Sn have been plotted in Figs. 11 and 12, along with the experimental data wherever appropriate. The low-temperature distortion and the matrix-element variation length $1/g$ [Eq. (17)] have been calculated by fitting the elastic constant ($c_{11}-c_{12}$) above the transition temperature to the experimental results.

The general agreement between theory and experiment is good, considering that there are very few adjustable parameters and the susceptibility (within a constant) specific-heat jump at the transition and the low-temperature tetragonal deformations have been predicted after all parameters have been fixed by other data. The background term in susceptibility is attractively small, unlike that of a previous attempt²⁰ on the basis of a step-function density of states which had two adjustable parameters (enhancement and a large background) and was still unable to fit elastic constant and susceptibility with the same parameters. Variation of T_m with B -site alloying on the basis of the rigid-band approximation is similar to that shown in Fig. 5(c) for the idealized model, which allows for quite a few percent alloying in Nb_3Sn before the martensitic transition is suppressed.

However, it is apparent from Table II that while the fit for V_3Si is very good, that for Nb_3Sn is not as satisfactory.²⁹ Firstly the susceptibility variation in Nb_3Sn is much smaller than predicted by theory. The sample studied had a rather broad maximum in the susceptibility, 10 K above the transition; a better sample, while giving a sharper peak, is not likely to remove discrepancy between theory and experiment entirely. Putting in electron-electron enhancement factors will only worsen the fit. Secondly, the observed low-temperature

TABLE II. Summary of results for V₃Si and Nb₃Sn.

Compound	Tight-binding parameters (eV)	Electron-phonon coupling parameter λ	Bare density of states N(E _F) elec/eV atom	$\left \frac{d\chi}{dT} \right _{T_c}$	$\chi(T_c) - \chi(T_c^0)$ (10 ⁻⁴ emu/g)	$\chi(T_c)$ (10 ⁻⁴ emu/g)	Specific heat jump at T _c , ΔC _p (J/mole K)	Coefficient of linear term in specific heat at low temperatures $\gamma_T = C_p(T)/T$ (mJ/g-atom K ²)	Zero temperature distortion $\epsilon = 10^3 c/a - 1 $	Jahn-Teller splitting at M point at T = 0	Peierls gap at X point $2\Delta_X(0)$ (K)		
												10 ⁻⁶ emu/g K	10 ⁻⁴ emu/g
V ₃ Si	Case I	β = -0.165 γ = 0.014	5.8	0.032	1.8	0.4	0.4	25 ^a	2.9 ^b	1.9	3.8	110	123
	Case II	β = -0.28 γ = 0.015	4.7	0.036	3.1	0.6	0.55	17 ^a	3.2 ^b	2.1	2.3	120	125
	Expt.	0.036 ^d	...	0.2 ^d	0.4 - 0.5 ^{4*}	17, 19 ^{5d}	2.2 - 2.4 ^f	2.2 - 2.4 ^f
Nb ₃ Sn	Case I	β = -0.25 γ = 0.021	3.9	0.0096	0.35	0.3	0.9	19 ^a	5.4 ^b	5.0	3.0	250	275
	Case II	β = -0.17 γ = 0.021	4.2	0.0092	-0.2	0.1	0.35	21 ^a	4.3 ^b	4.0	5.0	225	250
	Expt.	0.005 ^e	...	0.2 ^e	1.5 - 3.5 ^b	12 ^g , 17 ^h , 16 ^k	6.2 ^j	6.2 ^j

^a Includes only the two bands under consideration.
^b Does not include suppression due to onset of super conductivity; consequently the experimental figure is better compared with $\epsilon(T_c)$.
^c Reference 25.
^d Reference 19.
^e Reference 18.
^f Reference 24.
^g Reference 27.

^h Reference 19.
ⁱ Reference 26.
^j Reference 24.
^k Reference 27.

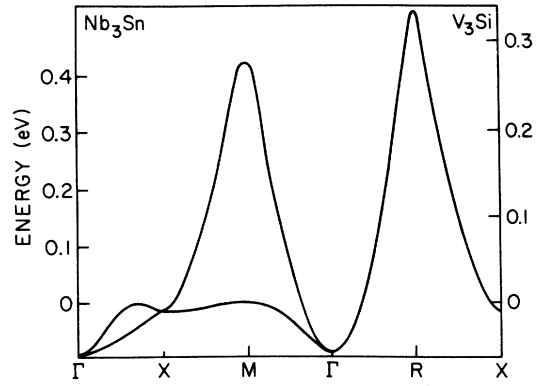


FIG. 9. Two relevant tight-binding bands for case I in Nb₃Sn and V₃Si (energy scales on left and right, respectively).

distortion is larger than that predicted by theory by (20–30)%. In this connection, however, it should be pointed out that the present results are better than those of Gor'kov¹³ or the Peierls transition model.¹⁴ Also the calculated specific-heat jump at the transition for Nb₃Sn is much too small, though the experimental data¹⁹ are not very good. Furthermore, for both V₃Si and Nb₃Sn the fits are better for a density of states somewhat [(10–30)%] larger than that calculated on the basis of specific data, though the latter analysis is not very reliable and subject to some controversy.

It is not possible in the present model to simultaneously remedy all these discrepancies in Nb₃Sn. The susceptibility is indicative of a lower density of states, or a wider peak, but such a change would

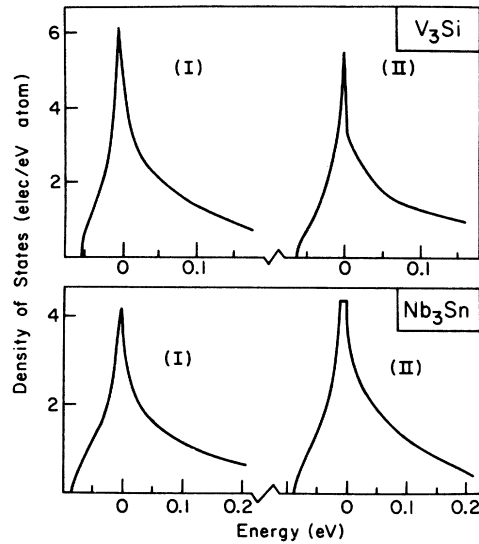


FIG. 10. Electronic density of states for the two cases in both V₃Si and Nb₃Sn.

reduce the calculated tetragonal distortion further [alternatively, the calculated $(c_{11}-c_{12})$ would recover much slower above T_m] and lower the specific-heat jump at the transition. This is reminiscent of the situation in the layered transition-metal dichalcogenide $2H\text{-TaSe}_2$, where the charge-density-wave gap and specific-heat jump are almost an order of magnitude larger than that predicted by a mean-field model with a BCS-type gap equation. This is because the coherence length at low temperatures in this compound is smaller than the superlattice spacing, and consequently phonons soften over a relatively large portion of the zone, and so a mean-field theory which does not include lattice entropy and local fluctuations will lead to incorrect results; one has to reformulate the problem in terms of local and global order parameters and include the entropy of the phonons in the calculation.³⁰ In the $A\text{-15}$ compounds the observed phonon softening is also over a large range of wave vectors, at least for the transverse wave in the $[110]$ direction. From a fit to the $[110]$ transverse $[\bar{1}\bar{1}0]$ polarized phonon dispersion curves,¹⁵ one obtains zero-temperature renormalized (experimentally observed) Landau-Ginzburg coherence lengths for Nb_3Sn and V_3Si as $0.64a_0$ and $0.94a_0$, respectively (a_0 is the lattice spacing). The actual ratio of importance,³⁰ $\pi\xi/a_0$, is ~ 2 for Nb_3Sn and ~ 3 for V_3Si . This gives the recovery of the softening along the $[110]$ direction; there is further recovery as one deviates from that direction and one must really include that before computing the effects of phonon entropy. However,

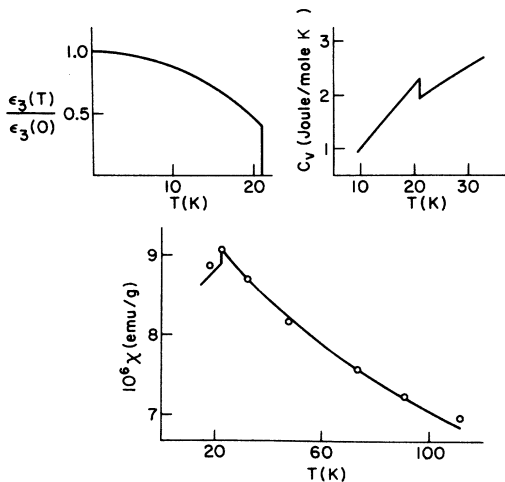


FIG. 11. Plots of the reduced tetragonal distortion, electronic specific heat, and susceptibility as functions of temperature for case I in V_3Si . Experimental data for magnetic susceptibility are from the later Ref. 21, normalized to the room-temperature values of the earlier Ref. 21.

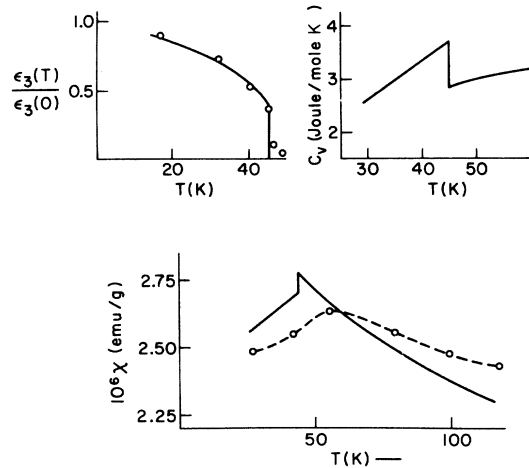


FIG. 12. Plots of the reduced tetragonal deformation, electronic specific heat, and magnetic susceptibility as functions of temperature for case I in Nb_3Sn . Experimental data on tetragonal distortion and magnetic susceptibility are from Refs. 28 and 20, respectively, and the dotted line is a smooth curve through the experimental points.

these numbers suggest that these compounds could be on the border line, where lattice entropy is presumably not important enough to radically change the results, but could account for larger zero-temperature distortions and specific-heat jump at the transition, and a somewhat lower density of states. Also the effect in Nb_3Sn where the softening extends to larger k should be more, as indeed seems to be the case.

Another simplification of the model is the assumed temperature independence of strong coupling effects, though this is probably not very important till about 100 K. Finally, of course, the model includes only the δ_1 subband; inclusion of other orbitals would change results somewhat, but it seems unlikely that the change would be sufficient to remedy the discrepancy in the heat-capacity jump at T_m . Further, it would introduce many more adjustable parameters which could not all be determined in any sensible manner.

One question which has so far been omitted from the discussion is the temperature variation of the shear modulus c_{44} . In the present model a pure shear strain along one of the cube edges does not cause a gap at the X point, nor does it shift the saddle points at M to first order; however, it does move the bands in the zone, and consequently causes change in the widths of the three contributions (corresponding to the fact that the cube has three symmetry directions) to the density of states. This would result in some softening which would essentially be smaller than $(c_{11}-c_{12})$ because it

is solely due to interchain coupling. While numerical fits have not been made, it is very likely that the slight c_{44} softening in V_3Si can be adequately explained; for Nb_3Sn the large softening seems to imply larger interchain coupling with a consequently smaller peak in the density of states—this seems to be consistent with the discussion on the effect of lattice entropy in Nb_3Sn . However, quantitative comparison can only be made when this effect is included, at least for Nb_3Sn .

VI. CONCLUDING REMARKS

The present work has tested a microscopic three-dimensional two-band tight-binding model of the *A-15* compounds based on Mattheiss' result that the density of states near the Fermi surface in the *A-15* compounds is composed mainly of the δ_1 orbitals on the transition-metal sites. The model has relatively few parameters, determined partly from Mattheiss' work and partly from experiment. For small interchain coupling, the model exhibits an instability of the electronic spectrum due in part to a Jahn-Teller effect and in part to a Peierls-like gap at the *X* point, and is capable of explaining the anomalies and structural instabilities observed in the *A-15* compounds.

The theory predicts the temperature variation of magnetic susceptibility, specific-heat jump at the transition, and low-temperature distortion for parameters determined by the electronic specific heat at low temperatures and the temperature variation of the elastic constant in the cubic phase. The results are in fairly good agreement with experiment and the inadequacies can be attributed to the role of lattice entropy which has been omitted in the present study. The susceptibility drop below the transition is in much better agreement with experiment than previous models.

One question of interest is the modification of the Landau theory of I and its results in light of the present work. Since the *X*-point Peierls gap is not the only or primary cause of the instability, the electronic order parameters ϕ_μ cannot be identified as the charge-density-wave amplitudes with $k = 2\pi/a$ in the *x*, *y*, and *z* directions. However, the success of the Landau theory of I leads to the belief that while it may not have been formulated on the basis of the correct microscopic model, its free-energy functional has the essential ingredients. The reason is not far to seek.

Recent work³¹ has shown that if one formulates a Landau theory based on a purely threefold degenerate Jahn-Teller model in which the electronic order parameters (corresponding to the motion of the three bands) are coupled with the

strain tensor as in the Labbe-Friedel model, the results of that phenomenological model are essentially those of I. The main difference is that there is no softening of the $\Gamma_{12}(+)$ optical mode.

The present model exhibits both effects—a threefold-degeneracy splitting (like the Labbe-Friedel model) and a Peierls gap (like the Gor'kov model). Thus a Landau theory based on the present model would have six electronic order parameters—three describing the motion of the threefold degeneracy of the bands corresponding to the three symmetry directions of the cubic lattice (such as the three *M* points or the three ΓX saddle points), and three others describing the *X*-point gaps. The first three would be coupled to the strain-tensor and the latter to the pairing optical modes. The results would be in between those of I and Ref. 31, but since those two agree in most respects, such a model would also yield results in agreement with experiment.

Secondly, the off-diagonal components of the strain tensor would also get coupled in, to the extent of interchain coupling, and show softening of c_{44} as experimentally observed. Of course, the value of the Fermi energy at which the transition temperature is maximum would not be the *X*-point energy but some other one. Finally, it would also explain why the magnetic susceptibility drop below the transition was incorrectly predicted¹⁷ on the basis of a simple Peierls model: because such a microscopic interpretation of the Landau theory parameters is inappropriate.

One difficulty faced by the Peierls-type interpretation of the Landau theory of I was the extremely small Fermi velocity $\sim 2 \times 10^6$ cm/sec (renormalized; bare value about twice as large) at the *X* point that resulted from the extremely short coherence length deduced from the phonon dispersion curves. The present model might be somewhat more successful in this regard³² as a substantial portion of the zone from *X* to *M* for the lower band and halfway from Γ to *X* for the upper band is reasonably flat, and all this portion takes part in the band motion which causes the instability.

In conclusion, the present model of the *A-15* compounds, based on a 3D band structure, seems to answer the need of a realistic microscopic picture of the *A-15* compounds. It is able to correlate many of the anomalies (magnetic susceptibility, specific heat, elastic constants) and the structural transition well in the case of V_3Si , and less adequately in Nb_3Sn (presumably because of the neglect of lattice entropy), and also seems to be promising in its ability to tie in other aspects of the phenomenon such as softening of the shear constant and phonon softening over a wide range of wave vectors, which is currently under in-

vestigation. As discussed earlier, it appears unlikely that another realistic (nonidealized) model of the transition which pictures it as being purely electronically driven, though based on another (perhaps 3D) band structure, would change the results in Nb_3Sn sufficiently to bring about total agreement. Further, such a model would have to be reasonably consistent with Mattheiss' calculations and also have a large portion of the band structure participating in the transition to explain the anomalously low coherence length. It therefore seems that the next step would be to work out a model system of coupled electrons and phonons which shows both instabilities of the electronic spectrum (Jahn-Teller, Peierls as well as superconducting) and significant phonon softening, including entropies of both systems. Further, in order to carry the calculations up to room temperature, strong coupling enhancement effects would have to be done self-consistently keeping in mind that the width of the density-of-states peak and the Debye temperature are comparable. This is clearly a formidable task so it may first be necessary to do this with idealized band structures or with approximations to the relevant portion of the band structure of the present model. Perhaps some general results regarding the interdependence of structural and superconducting instabilities may then emerge, providing a better view into the working of these high-temperature superconductors.

ACKNOWLEDGMENTS

The author is grateful to his advisor, Professor W. L. McMillan, for suggesting the above problem and for his suggestions and guidance from time to time during the course of the present study. Sincere thanks are due to Mark Sears whose eigenvalue routine was used for the diagonalization of the tight-binding matrix as a part of the computer calculation.

APPENDIX: DENSITY OF STATES AND RELATED QUANTITIES FOR LINEAR BANDS

In the case of bands which vary linearly, the constant-energy surfaces are a set of parallel planes to which the energy gradient forms the normal. Bands may be approximated in a "small enough" cubic region to vary linearly, except immediately in the vicinity of an extremum or a saddle point, and the density of states is just the area of the plane intercepted by the cube divided by the (constant) energy gradient within the cube.

The distance of the plane (characterized by E) from the center of the cube is given by

$$w = |E - E_c| / |\vec{\nabla}E|_c,$$

where E_c is the energy at the center of the cube. If the direction cosines of the plane are l_1, l_2, l_3 , with $l_1 \geq l_2 \geq l_3 \geq 0$ without loss of generality (this can be achieved by simply relabeling the axes), then define

$$w_1 = b |l_1 - l_2 - l_3|, \quad w_2 = b(l_1 - l_2 + l_3),$$

$$w_3 = b(l_1 + l_2 - l_3), \quad w_4 = b(l_1 + l_2 + l_3),$$

where $2b$ is the length of the cube. $w_1 - w_4$ are the distances, in increasing order, of the four corners lying in the half of the cube in which the plane lies, from the center of the cube.

Then the area of the plane intercepted by the cube is given by different formulas for different ranges of the distance w :

Case I: $w < w_1$. (a) If $l_1 > l_2 + l_3$, the cross section is a parallelogram of area

$$S = 4b^2/l_1.$$

(b) If $l_1 < l_2 + l_3$, the cross section is hexagonal with area

$$S(w) = \frac{2b^2(l_1l_2 + l_2l_3 + l_3l_1) - (w^2 + b^2)}{l_1l_2l_3}.$$

Case II: $w_1 < w < w_2$. The shape is a pentagon of area

$$S(w) = \frac{b^2(3l_2l_3 + l_1l_2 + l_3l_1) - bw(l_2 + l_3 - l_1) - \frac{1}{2}(w^2 + b^2)}{l_1l_2l_3}$$

Case III: $w_2 < w < w_3$. The cross section is a quadrilateral and

$$S(w) = 2[b^2l_3(l_1 + l_2) - bw l_3]/l_1l_2l_3.$$

Case IV: $w_3 < w < w_4$. The figure is a triangle of area

$$S(w) = [b(l_1 + l_2 + l_3) - w]^2/2l_1l_2l_3.$$

For $w > w_4$, of course, the plane does not intercept the cube and $S(w) = 0$.

The density of states and its derivatives are given by [omitting the factor $V/(2\pi)^3$]

$$N(E) = (1/|\vec{\nabla}E|)S(w),$$

$$N'(E) = (1/|\vec{\nabla}E|^2) \text{sgn}(E - E_c)S'(w),$$

$$N''(E) = (1/|\vec{\nabla}E|)S''(w).$$

While $N(E)$ and $N'(E)$ are continuous across the boundaries, $N''(E)$ is not, and therefore it should be "smoothed" over an appropriate range. The number of states below certain energy E , $n(E)$, is obtained by integrating $N(E)$ from $w = w_4$ to the appropriate point; for $E > E_c$, the result should be subtracted from $8b^3$, the volume of the cube. The results for $E < E_c$ are given below:

Case I: $w < w_1$.

(a) $l_1 > l_2 + l_3$, $n(E) = (4b^2/l_1)(bl_1 - w)$

(b) $l_1 < l_2 + l_3$,

$$n(E) = 4b^3 + \frac{w^3}{3l_1l_2l_3} - \frac{b^2w(2l_1l_2 + 2l_2l_3 + 2l_3l_1 - l_1^2 - l_2^2 - l_3^2)}{l_1l_2l_3}.$$

Case II: $w_1 < w < w_2$.

$$n(E) = \frac{4b^3}{3l_1l_2} [l_3^2 + 3l_2(l_2 - l_3)] + \frac{w_2 - w}{4l_1l_2l_3} [4b^2(3l_2l_3 + l_3l_1 + l_1l_2) - 2b^2 + b(w_2 + w)(l_1 - l_2 - l_3) - \frac{2}{3}(w_2^2 + ww_2 + w^2)].$$

Case III: $w_2 < w < w_3$.

$$n(E) = (b/3l_1l_2)[4b^2l_3^2 + 3(w_3 - w)(w_4 - w)].$$

Case IV: $w_3 < w < w_4$.

$$n(E) = (w_4 - w)^3/6l_1l_2l_3.$$

*Most of this work is based on a thesis submitted in partial fulfillment of the requirements for the degree of Ph.D. in Physics in the Graduate College of the University of Illinois at Urbana-Champaign, where it was supported in part by NSF Contract No. DMR 75-20376.

†Supported by IBM Fellowship while at the University of Illinois.

‡Present address.

¹B. W. Batterman and C. S. Barrett, Phys. Rev. Lett. **13**, 390 (1964); Phys. Rev. **149**, 296 (1966).

²M. Weger and I. B. Goldberg, in *Solid State Physics*, edited by H. Ehrenreich, F. Seitz, and D. Turnbull (Academic, New York, 1973), Vol. 28, p. 1.

³L. R. Testardi, in *Physical Acoustics*, edited by W. P. Mason and R. N. Thurston (Academic, New York, 1973), Vol. X, p. 193; L. R. Testardi, Rev. Mod. Phys. **47**, 637 (1975).

⁴Yu. A. Izyumov and Z. Z. Kurmaev, Usp. Fiz. Nauk. **113**, 193 (1974) [Sov. Phys.-Usp. **17**, 356 (1974)].

⁵L. P. Gor'kov (unpublished).

⁶J. Labbe and J. J. Friedel, J. Phys. Radium **27**, 708 (1966).

⁷R. W. Cohen, C. D. Cody, and J. J. Halloran, Phys. Rev. Lett. **19**, 840 (1967).

⁸L. J. Sham, Phys. Rev. Lett. **27**, 1725 (1971); J. Noolandi and L. J. Sham, Phys. Rev. B **8**, 2468 (1973).

⁹E. Pytte, Phys. Rev. Lett. **25**, 1176 (1970).

¹⁰B. M. Klein and J. L. Birman, Phys. Rev. Lett. **25**, 1014 (1970).

¹¹L. F. Mattheiss, Phys. Rev. **138**, A112 (1965); Phys. Rev. B **12**, 2161 (1975).

¹²L. P. Gor'kov, Pis'ma Zh. Eksp. Teor. Fiz. **17**, 525 (1973) [JETP Lett. **17**, 379 (1973)]; Zh. Eksp. Teor. Fiz. **65**, 1658 (1973) [Sov. Phys.-JETP **38**, 830 (1974)].

¹³L. P. Gor'kov and O. N. Dorokhov, J. Low Temp. Phys. **22**, 1 (1976); Pis'ma Zh. Eksp. Teor. Fiz. **21**, 656 (1975) [JETP Lett. **21**, 310 (1975)].

¹⁴R. N. Bhatt, Ph.D. thesis (University of Illinois, 1976) (unpublished).

¹⁵R. N. Bhatt and W. L. McMillan, Phys. Rev. B **14**, 1007 (1976).

¹⁶Griff Bilbro and W. L. McMillan, Phys. Rev. B **14**, 1887 (1976).

¹⁷Reference 15 contains an error of a factor of 4 in Sec. VII G; instead of being larger by 20%, the theoretical drop in susceptibility is too large by a factor of 5.

¹⁸J. C. F. Brock, Solid State Commun. **7**, 1789 (1969).

¹⁹L. J. Vieland and A. W. Wicklund, Solid State Commun. **7**, 37 (1969).

²⁰W. Rehwald, M. Rayl, R. W. Cohen, and G. D. Cody, Phys. Rev. B **6**, 363 (1972).

²¹H. J. Williams and R. C. Sherwood, Bull. Am. Phys. Soc. **5**, 430 (1960); J. P. Maita and E. Bucher, Phys. Rev. Lett. **29**, 931 (1972).

²²G. Gilat and L. J. Raubenheimer, Phys. Rev. **144**, 390 (1966).

²³W. L. McMillan, Phys. Rev. **167**, 331 (1968).

²⁴G. Shirane and J. D. Axe, Phys. Rev. B **4**, 2957 (1971).

²⁵G. S. Knapp, S. D. Bader, H. V. Culbert, F. Y. Fradin, and T. E. Klippert, Phys. Rev. B **11**, 4331 (1975); G. S. Knapp, S. D. Bader, and Z. Fisk, Phys. Rev. B **13**, 3783 (1976).

²⁶L. J. Vieland and A. W. Wicklund, Phys. Rev. **166**, 424 (1968).

²⁷F. J. Morin and J. P. Maita, Phys. Rev. **129**, 1115 (1965).

²⁸L. J. Vieland, R. W. Cohen, and W. Rehwald, Phys. Rev. Lett. **26**, 373 (1971).

²⁹With reference to Nb₃Sn, it should be mentioned that the value of λ used from Ref. 25 is somewhat lower than the values given by other measurements. Using those values of λ would mean a (15–20)% increase in $1 + \lambda$ and one would then need to use slightly larger tight-binding parameters to get a lower bare density of states. For the present model the variation in susceptibility and other results would not be altered significantly. However, the variation of the strong coupling renormalization factor with temperature would then be more important and may play a role too.

³⁰W. L. McMillan, Phys. Rev. B **16**, 643 (1977).

³¹R. N. Bhatt (unpublished).

³²Preliminary results by R. N. Bhatt and P. A. Lee (unpublished) show that this is the case.

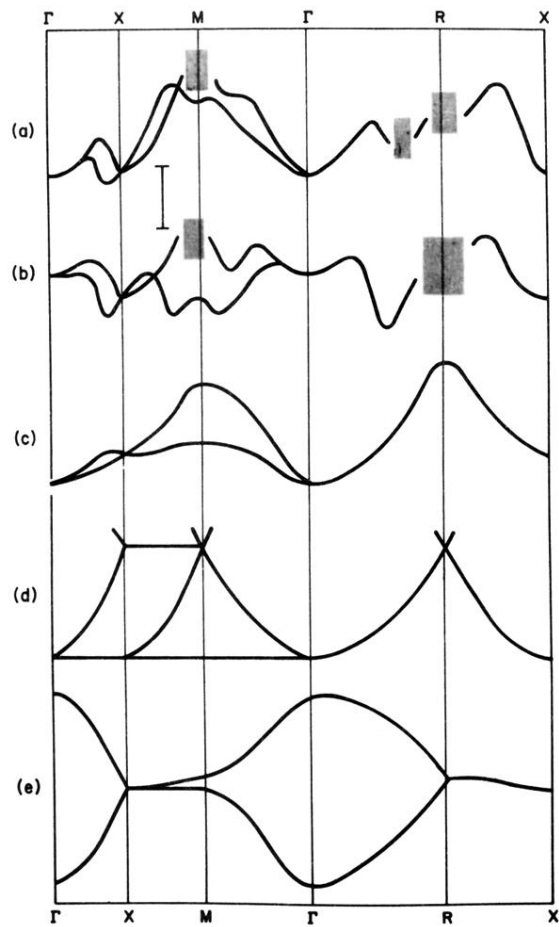


FIG. 7. Two bands near the Fermi surface in Mattheiss, calculation for Nb_3Sn (a) and V_3Si (b), along with the bands used in the present calculation (c), the Labbe-Friedel model (d), and the Gor'kov model (e), drawn roughly to scale. The shaded area in Mattheiss' band represents presence of other bands (and consequent mixing), and his rms error is indicated by I.